

Realizing Rec. 2020 color gamut with quantum dot displays

Ruidong Zhu,¹ Zhenyue Luo,¹ Haiwei Chen,¹ Yajie Dong,^{1,2} and Shin-Tson Wu^{1,*}

¹CREOL, The College of Optics and Photonics, University of Central Florida, Orlando, Florida 32816, USA

²NanoScience Technology Center, University of Central Florida, Orlando, Florida 32826, USA

*swu@ucf.edu

Abstract: We analyze how to realize Rec. 2020 wide color gamut with quantum dots. For photoluminescence, our simulation indicates that we are able to achieve over 97% of the Rec. 2020 standard with quantum dots by optimizing the emission spectra and redesigning the color filters. For electroluminescence, by optimizing the emission spectra of quantum dots is adequate to render over 97% of the Rec. 2020 standard. We also analyze the efficiency and angular performance of these devices, and then compare results with LCDs using green and red phosphors-based LED backlight. Our results indicate that quantum dot display is an outstanding candidate for achieving wide color gamut and high optical efficiency.

©2015 Optical Society of America

OCIS codes: (250.5590) Optoelectronics: Quantum-well, -wire and -dot devices; (330.1715) Color, rendering and metamerism; (230.3670) Light-emitting diodes; (230.3720) Liquid-crystal devices.

References and links

1. Adobe Systems Inc., “Adobe RGB (1998) color image encoding,” 2005.
2. SMPTE RP 431–2, “D-cinema quality — reference projector and environment,” 2011.
3. ITU-R Recommendation BT.709–5, “Parameter values for the HDTV standards for production and international programme exchange,” 2002.
4. ITU-R Recommendation BT.2020, “Parameter values for ultra-high definition television systems for production and international programme exchange,” 2012.
5. K. Masaoka, Y. Nishida, M. Sugawara, and E. Nakasu, “Design of primaries for a wide-gamut television colorimetry,” *IEEE Trans. Broadcast* **56**(4), 452–457 (2010).
6. M. R. Pointer, “The gamut of real surface colours,” *Color Res. Appl.* **5**(3), 145–155 (1980).
7. K. Masaoka, Y. Nishida, and M. Sugawara, “Designing display primaries with currently available light sources for UHD TV wide-gamut system colorimetry,” *Opt. Express* **22**(16), 19069–19077 (2014).
8. K. V. Chellappan, E. Erden, and H. Urey, “Laser-based displays: A review,” *Appl. Opt.* **49**(25), F79–F98 (2010).
9. S. Kim, S. H. Im, and S.-W. Kim, “Performance of light-emitting-diode based on quantum dots,” *Nanoscale* **5**(12), 5205–5214 (2013).
10. Z. Luo, Y. Chen, and S.-T. Wu, “Wide color gamut LCD with a quantum dot backlight,” *Opt. Express* **21**(22), 26269–26284 (2013).
11. Z. Luo, D. Xu, and S.-T. Wu, “Emerging quantum-dots-enhanced LCDs,” *J. Display Technol.* **10**(7), 526–539 (2014).
12. X. Dai, Z. Zhang, Y. Jin, Y. Niu, H. Cao, X. Liang, L. Chen, J. Wang, and X. Peng, “Solution-processed, high-performance light-emitting diodes based on quantum dots,” *Nature* **515**(7525), 96–99 (2014).
13. Y. Dong, J.-M. Caruge, Z. Zhou, C. Hamilton, Z. Popovic, J. Ho, M. Stevenson, G. Liu, V. Bulovic, M. Bawendi, P. T. Kazlas, J. Steckel, and S. Coe-Sullivan, “Ultra-bright, highly efficient, low roll-off inverted quantum-dot light emitting devices (QLEDs),” *SID Symp. Dig. Tech. Pap.* **46**(1), 270–273 (2015).
14. Y. Yang, Y. Zheng, W. Cao, A. Titov, J. Hyvonen, J. R. Manders, J. Xue, P. H. Holloway, and L. Qian, “High-efficiency light-emitting devices based on quantum dots with tailored nanostructures,” *Nat. Photonics* **9**(4), 259–266 (2015).
15. H. Shen, W. Cao, N. T. Shewmon, C. Yang, L. S. Li, and J. Xue, “High-efficiency, low turn-on voltage blue-violet quantum-dot-based light-emitting diodes,” *Nano Lett.* **15**(2), 1211–1216 (2015).
16. K. Masaoka and Y. Nishida, “Metric of color-space coverage for wide-gamut displays,” *Opt. Express* **23**(6), 7802–7808 (2015).
17. M. Reyes-Sierra and C. A. C. Coello, “Multi-objective particle swarm optimizers: a survey of the state-of-the-art,” *Int. J. Comput. Intell. Res.* **2**, 287–308 (2006).

18. J. S. Steckel, J. Ho, C. Hamilton, C. Breen, W. Liu, P. Allen, J. Xi, and S. Coe-Sullivan, "12.1: Invited paper: Quantum dots: the ultimate down-conversion material for LCD displays," *SID Symp. Dig. Tech. Pap.* **45**(1), 130–133 (2014).
19. J. Chen, V. Hardev, J. Hartlove, J. Hofler, and E. Lee, "66.1: Distinguished paper: A high-efficiency wide-color-gamut solid-state backlight system for LCDs using quantum dot enhancement film," *SID Symp. Dig. Tech. Pap.* **43**(1), 895–896 (2012).
20. M. Schadt, "Milestone in the history of field-effect liquid crystal displays and materials," *Jpn. J. Appl. Phys.* **48**(3), 03B001 (2009).
21. C. A. C. Coello and G. B. Lamont, *Applications of Multi-Objective Evolutionary Algorithms* (World Scientific, 2004).
22. J. S. Steckel, R. Colby, W. Liu, K. Hutchinson, C. Breen, J. Ritter, and S. Coe-Sullivan, "68.1: Invited paper: Quantum dot manufacturing requirements for the high volume LCD market," *SID Symp. Dig. Tech. Pap.* **44**(1), 943–945 (2013).
23. J.-J. Lyu, J. Sohn, H. Y. Kim, and S. Lee, "Recent trends on patterned vertical alignment (PVA) and fringe-field switching (FFS) liquid crystal displays for liquid crystal television applications," *J. Display Technol.* **3**(4), 404–412 (2007).
24. H. Chen, M. Hu, F. Peng, J. Li, Z. An, and S.-T. Wu, "Ultra-low viscosity liquid crystal materials," *Opt. Mater. Express* **5**(3), 655–660 (2015).
25. S. H. Lee, S. L. Lee, and H. Y. Kim, "Electro-optic characteristics and switching principle of a nematic liquid crystal cell controlled by fringe-field switching," *Appl. Phys. Lett.* **73**(20), 2881–2883 (1998).
26. H. Chen, Z. Luo, D. Xu, F. Peng, S.-T. Wu, M.-C. Li, S.-L. Lee, and W.-C. Tsai, "A fast-response A-film-enhanced fringe field switching liquid crystal display," *Liq. Cryst.* **42**(4), 537–542 (2015).
27. H. Zhan, Z. Xu, C. Tian, Y. Wang, M. Chen, W. Kim, Z. Bu, X. Shao, and S. Lee, "Achieving standard wide color gamut by tuning led backlight and color filter spectrum in LCD," *J. Soc. Inf. Disp.* **22**(11), 545–551 (2014).
28. J. Chen, S. Gensler, J. Hartlove, J. Yurek, E. Lee, J. Thielen, J. Van Derlofske, J. Hillis, G. Benoit, J. Tibbit, and A. Lathrop, "Quantum dots: optimizing LCD systems to achieve Rec. 2020 color performance," *SID Symp. Dig. Tech. Pap.* **46**(1), 173–175 (2015).
29. J. M. Hillis, J. Thielen, J. Tibbits, A. Lathrop, D. Lamb, and J. Van Derlofske, "Closing in on Rec. 2020 – how close is close enough?" *SID Symp. Dig. Tech. Pap.* **46**(1), 223–226 (2015).
30. R. Zhu, Z. Luo, and S.-T. Wu, "Light extraction analysis and enhancement in a quantum dot light emitting diode," *Opt. Express* **22**(S7 Suppl 7), A1783–A1798 (2014).
31. K. A. Neyts, "Simulation of light emission from thin-film microcavities," *J. Opt. Soc. Am. A* **15**(4), 962–971 (1998).
32. H. Liang, R. Zhu, Y. Dong, S.-T. Wu, J. Li, J. Wang, and J. Zhou, "Enhancing the outcoupling efficiency of quantum dot LEDs with internal nano-scattering pattern," *Opt. Express* **23**(10), 12910–12922 (2015).
33. R. Lu, Q. Hong, Z. Ge, and S.-T. Wu, "Color shift reduction of a multi-domain IPS-LCD using RGB-LED backlight," *Opt. Express* **14**(13), 6243–6252 (2006).
34. Y.-L. Chen, J.-C. Hsiang, Y.-H. Wu, and C.-L. Yang, "P-118: Multi-domain fringe-field switched mobile LCD for reducing color shift by zigzag-like pixel design," *SID Symp. Dig. Tech. Pap.* **41**(1), 1709–1712 (2010).
35. S.-S. Park, I. Sohn, E. Cho, S. Park, and E. Kim, "Color shift reduction of liquid crystal displays by controlling light distribution using a micro-lens array film," *J. Display Technol.* **8**(11), 643–649 (2012).
36. S. Hofmann, M. Thomschke, P. Freitag, M. Furno, B. Lüsse, and K. Leo, "Top-emitting organic light-emitting diodes: Influence of cavity design," *Appl. Phys. Lett.* **97**(25), 253308 (2010).
37. Y. Ito, T. Hori, H. Tani, Y. Ueno, T. Kusunoki, H. Nomura, and H. Kondo, "59.1: A backlight system with a phosphor sheet providing both wider color gamut and higher efficiency," *SID Symp. Dig. Tech. Pap.* **44**(1), 816–819 (2013).
38. P. Li, Z. Wang, Q. Guo, and Z. Yang, "Luminescence and energy transfer of 432 nm blue LED radiation-converting phosphor $\text{Ca}_2\text{Y}_6\text{O}(\text{SiO}_4)_6:\text{Eu}^{2+}, \text{Mn}^{2+}$ for warm white LEDs," *RSC Advances* **5**(6), 4448–4453 (2015).
39. E. Jang, S. Jun, H. Jang, J. Lim, B. Kim, and Y. Kim, "White-light-emitting diodes with quantum dot color converters for display backlights," *Adv. Mater.* **22**(28), 3076–3080 (2010).
40. R. L. Donofrio, "Review paper: The Helmholtz-Kohlrausch effect," *J. Soc. Inf. Disp.* **19**(10), 658–664 (2011).
41. J. F. Van Derlofske, J. M. Hillis, A. Lathrop, J. Wheatley, J. Thielen, and G. Benoit, "19.1: Invited paper: Illuminating the value of larger color gamuts for quantum dot displays," *SID Symp. Dig. Tech. Pap.* **45**(1), 237–240 (2014).

1. Introduction

Wide color gamut enables a display device to represent the real object accurately. Several standards have been proposed to regulate how a display should reproduce colors, such as the Adobe RGB [1], SMPTE RP 431-2 for digital cameras [2], Rec.709 for high definition TVs [3], and Rec. 2020 for ultra-high definition (UHD) TVs [4]. The color gamut of these standards are defined by their corresponding RGB primaries; especially the color gamut of Rec. 2020 can enclose that of all the other three standards [5]. Meanwhile, the color triangle

of Rec. 2020 can cover up to 99.9% of the Pointer's gamut [6], which indicates displays capable of handling Rec. 2020 can faithfully reproduce the natural object colors. Finally yet importantly, the Rec. 2020 standard can be physically realized through RGB laser sources [5, 7].

Although the Rec. 2020 standard can be realized with monochromatic laser sources, for a real display, laser sources are expensive and the speckle problem [8] has not yet been fully solved. In this sense, it is preferred to find non-monochromatic light sources to realize the Rec. 2020 standard. Among these candidates, quantum dots (QDs) have attracted much attention because of their narrow and tunable emission spectra [9].

There are two approaches to use QDs for displays: photoluminescence (PL) quantum dots for liquid crystal display (LCD) backlight [10, 11] and electroluminescence (EL) quantum-dot light emitting diodes (QLEDs) [12–15]. In this paper, we will discuss how to realize the Rec. 2020 standards with both approaches, and the tradeoff between color gamut and optical efficiency.

2. Display system evaluation

Before we dive into performance evaluation of different displays, we should first establish the evaluation metrics. The first evaluation metric is color gamut, which is determined by the maximum colors a display can reproduce based on Rec. 2020. While the system colorimetry of Rec. 2020 [4] shown in Table 1 is quite straightforward, the definition of color gamut is sometimes confusing and misleading. Some manufactures define the area ratio as the color gamut, which compares the RGB triangular area of a display with the triangular area of the Rec. 2020 standard, namely:

$$\text{Color Gamut Area} = \frac{A_{\text{display}}}{A_{\text{standard}}}, \quad (1)$$

but others define the coverage ratio as the color gamut, which can be expressed as:

$$\text{Color Gamut Coverage} = \frac{A_{\text{display}} \cap A_{\text{standard}}}{A_{\text{standard}}}. \quad (2)$$

What makes the situation even more confusing is that CIE 1931 and CIE 1976 are used simultaneously when calculating the color gamut, although these two color spaces are quite different. As pointed out in [16], the coverage ratios in CIE 1931 and CIE 1976 are rather inconsistent, and the coverage ratio calculated with CIE 1931 is more consistent to the Rec. 2020 volume coverage ratio in color appearance model CIELAB, CIELUV and CIECAM02. In this sense, we will use the coverage ratio in CIE 1931 as the metric, while including the coverage ratio in CIE 1976 as a reference. We will discuss more about the color space selection in Sec. 5.

Table 1. System colorimetry of Rec. 2020 standard

Primary colors and Reference white	Chromaticity coordinates (CIE 1931)	x	y	Corresponding wavelength (nm)
	Red Primary		0.708	0.292
Green Primary		0.170	0.797	532
Blue Primary		0.131	0.046	467
Reference White (D65)		0.313	0.329	/

The other metric should describe how efficient the display system is. Here we emphasize on optical efficiency because realizing a wide color gamut is mainly to optimize the output

spectra power density (SPD). The SPD directly determines the luminous efficacy of radiation (*LER*) of the system [10]:

$$LER = \frac{K_m \int S_{out}(\lambda) V(\lambda) d\lambda}{\int S_{out}(\lambda) d\lambda}. \quad (3)$$

In Eq. (3), $S_{out}(\lambda)$ is the SPD of the output light, $V(\lambda)$ is the standard luminosity function, and $K_m = 683 \text{ lm/W}$ is the *LER* of the ideal monochromatic 555-nm source. As the *LER* is only determined by the light spectra, it sets the theoretical limit for the total efficiency of a display.

For a non-emissive display such as LCD, the SPD of the backlight ($S_{in}(\lambda)$) and the actual output light ($S_{out}(\lambda)$) can be modulated dramatically, depending on the transmission characteristics of the system. To quantify the transmission characteristics of the system, we introduce the transfer efficiency (*TE*) of the system as:

$$TE = \frac{\int S_{out}(\lambda) d\lambda}{\int S_{in}(\lambda) d\lambda}. \quad (4)$$

The total light efficiency (*TLE*) of the system is:

$$TLE = LER \cdot TE = \frac{K_m \int S_{out}(\lambda) V(\lambda) d\lambda}{\int S_{in}(\lambda) d\lambda}. \quad (5)$$

For our analysis below, the main evaluation metrics are color gamut and *LER*. While evaluating a non-emissive display, we will also discuss its *TLE*.

The evaluation process can be outlined as follows: assuming a display with RGB primary colors, the SPD of each primary color can be written as $S_{out,i}(\lambda)$ ($i = r, g, b$), and the total output light spectra reaching the system white point is:

$$S_{out}(\lambda) = RS_{out,r}(\lambda) + GS_{out,g}(\lambda) + BS_{out,b}(\lambda), \quad (6)$$

$$R + G + B = 1.$$

In Eq. (6), R, G and B represent the weighting ratio of the corresponding color; they are so determined that the white point of the display is D65.

For both PL and EL QDs, the normalized SPD of a single color fits well with the Gaussian function:

$$S_i(\lambda, \lambda_0, \Delta\lambda) = e^{-4 \ln 2 \frac{(\lambda - \lambda_0)^2}{\Delta\lambda^2}}, \quad (7)$$

here i stands for R, G and B, respectively, λ_0 is the central wavelength, and $\Delta\lambda$ is the linewidth of the emission spectra (full width half maximum).

With Eqs. (2)-(7), we can calculate the color gamut and *LER* of the display, and for a non-emissive display, we can also calculate the *TLE* of the system. We can then optimize the color gamut by varying the QD's central wavelength λ_0 and linewidth $\Delta\lambda$. Several approaches have been developed to optimize the color gamut of a display; the most convenient one is the multi-objective optimization that combines both *LER* (*TLE*) and color gamut. The detailed approach has been described in [10, 17], and the results will be discussed later.

As an example, we calculate the *LER* of an ideal laser display with three monochromatic light sources, which covers 100% color gamut of Rec. 2020. The resultant R, G and B are 39.7%, 30.8% and 29.5%, respectively, and *LER* is 273.9 lm/W. This *LER* serves as benchmark for our comparison.

3. Wide color gamut QD-enhanced LCD

Recently, QD-enhanced LCDs are emerging. Contemporary QD-LCDs use either on-edge approach [18] where the quantum dot is placed on the edge of the light guide plate or film approach [19] where the quantum dots are embedded in an optical film on top of the light guide plate. For these two approaches, they both use a blue LED to pump the red and green quantum dots. The generated light is modulated by the LC layer (sandwiched between crossed polarizers), and passes through the color filters (CFs). Besides the spectra of the backlight, the color of the display can be affected by the transmittance of the color filters and the wavelength dispersion of the LC material and polarizers. However, in comparison with color filters, the dispersion of the LC material and polarizers has negligible effect on the color performance [20]. This is because for different LC modes, although the overall transmittance slightly depends on the wavelength, the shape of these transmission curves remain quite similar [10]. If we consider the transmittance of the RGB color filters and the LC, we can say that the color filters play the major role in terms of reshaping the output light spectra. The LC materials we use here are the same as [10].

Next, we examine how to achieve wide color gamut with two commercial color filters: CF1 is commonly used for TVs because of its relatively high transmittance, especially for green and blue. However, the crosstalk between different channels is larger than that of CF2, as shown in Fig. 1(a). Obviously, it will be more difficult to obtain wide color gamut with CF1. To confirm this and see how wide a color gamut we can get, we plot the Pareto front [21] of the LCD with these two CFs and for two commonly used LC modes: n-FFS for mobile displays and MVA for large-size TVs. The Pareto front determines the optimal value of a display and all the solutions will fall either on or below the Pareto Front.

Contemporary Cd-based QDs usually have a linewidth between 20~30nm [22], and thus it is plausible to select 20nm and 30nm as the boundary conditions for linewidth. Meanwhile, for LCD applications, the blue part is achieved through blue LED and its linewidth is about 20nm. Because of this reason, the two boundary conditions for RGB QD-LCD in terms of linewidth are 1) $\Delta\lambda_r = \Delta\lambda_g = 30\text{nm}$, $\Delta\lambda_b = 20\text{nm}$; and 2) $\Delta\lambda_r = \Delta\lambda_g = \Delta\lambda_b = 20\text{nm}$. We then vary the central wavelength λ_0 and the R, G, B ratios. All the results below are calculated in the CIE 1931 chromaticity diagram and the reference white point is always D65. Of course, we can also set the linewidth of the R, G and B colors as variables to match the Rec. 2020 color gamut, and these Pareto fronts will fall between the two boundaries. These results will be discussed later in Sec. 4.

Figure 1(b) depicts the simulated Pareto Front: the solid lines represent the upper-limit, i.e. the linewidth is 20nm for R, G and B colors, whereas the dashed lines represent the lower-limit boundary conditions where the linewidth is 30nm for red and green, and 20nm for blue. The red and green lines in Fig. 1(b) represent the n-FFS mode whereas the blue and black lines represent the MVA mode. The red and blue lines use CF1 while green and black lines use CF2. From Fig. 1(b) we can deduce that 1) wider color gamut always trades off with lower TLE. 2) Even though the color gamut is jointly determined by the CFs, the transmittance of the LC cell, and the linewidth of the primaries, their importance is different. The CFs play the most important role while the transmittance of the LC cell is least important. In the meantime, a light source with narrower linewidth (red and green QDs and blue LED) helps widen the color gamut. 3) Comparing the red solid line with the blue solid line, the transmittance of the LC has little to do with the color gamut. However, different LC modes can dramatically affect the TLE of the system. For the n-FFS mode, its average TLE is 27.4 while for the MVA mode its average TLE is 18.7, which is quite close to the transmittance difference of the n-FFS and MVA modes (95% vs. 70%). 4) Comparing CF1 with CF2, displays with CF1 usually have higher TLE, but it is difficult to get wide color gamut. For n-FFS, the widest color gamut we can get with CF1 and CF2 are summarized in Figs. 1(c) and 1(d) and Table 2 (the linewidths of the three colors are all 20nm). In the

meantime, we can clearly see that in comparison with CF1, CF2 sacrifices 24% *TLE* but only gain 2.7% in color gamut. This tradeoff is not worth taking. For MVA, the results are quite similar except that the *TLE* is lower. The reason that MVA has a lower *TLE* than n-FFS is due to its relatively large electrode size (for TVs), as a result, the dead zone area is larger [23], which in turn lowers the transmittance. While for n-FFS (for smart phones), its transmittance can reach 95% [24–26].

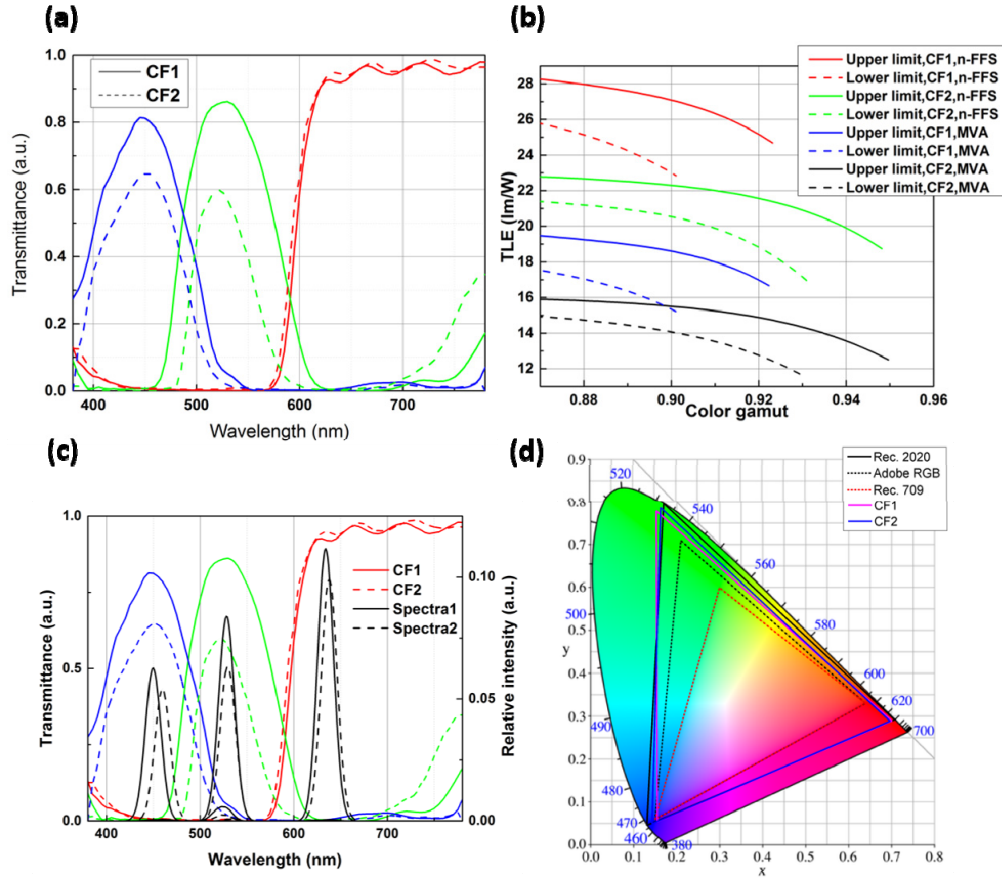


Fig. 1. (a) The transmittance of two color filters; (b) the *Pareto* front of the QD-LCDs with different boundary condition, LC mode and color filters; (c) the transmittance and the corresponding optimized output spectra for the two color filters; and (d) the simulated color gamut for the two optimized output spectra.

From Figs. 1(c) and 1(d), the red primary is quite close to the Rec. 2020 standard, while the green and blue primaries still fall short, especially the green. This results from the crosstalk between green and blue color filters. There are two approaches to resolve this problem: 1) reducing the linewidth of the QD and blue LED further, and 2) redesigning the color filters.

Table 2. Optimized values of the two wide color gamut n-FFS LCDs with CF1 and CF2, respectively.

CF type	CF1	CF2
<i>TLE</i> (lm/W)	24.6	18.7
Color Gamut	92.3%	94.8%

In the first approach, let us make a bold assumption that the linewidth of the three primary colors can be further reduced to 10nm, which has not been achieved by commercial materials yet. Table 3 lists the simulated results. We find that even with such a narrowband light source, the color gamut improvement is insignificant because of the crosstalk between different color filters. A more promising approach is to narrow the bandwidth of color filters.

Table 3. Optimized values of two wide color gamut MVA LCDs with 10-nm-linewidth primary colors for CF1 and CF2, respectively.

CF type	CF1	CF2
<i>TLE</i> (lm/W)	17.6	13.3
Color Gamut	94.1%	96.0%

Several approaches have been proposed to reduce the crosstalk between different color channels [27, 28]. Figure 2(a) shows one of the newly proposed color filters [28]: the red color filter is optimized to reduce the long transmission tail at the blue-green region. However, the crosstalk between green and blue color filters is still quite severe. Designing an even wider color gamut QD-LCD is tricky for two reasons: 1) Of course we can enlarge the color gamut by using deeper blue and red, or shifting the cutoff wavelength of the color filters, however, these do not necessarily mean large color gamut coverage as the area might overlap less with the Rec. 2020 standard. Thus predicting the color gamut is more difficult. 2) The white point has to occur at D65, which gives us less design freedom.

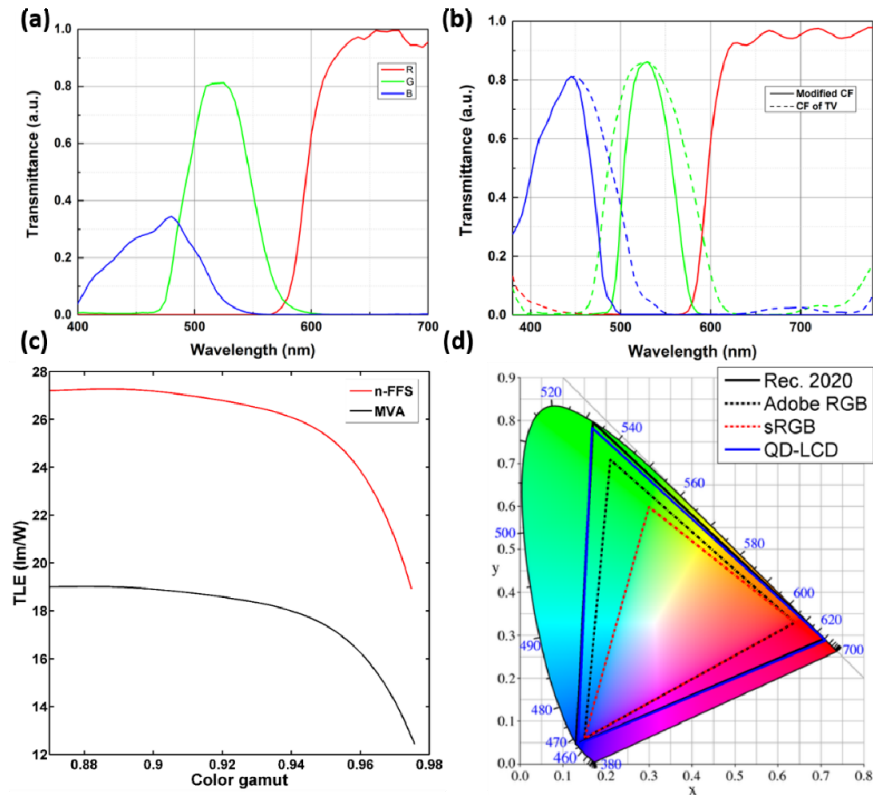


Fig. 2. (a) One of the proposed CFs with wide color gamut. (b) The transmittance of our modified CFs based on the CFs for TV. (c) The *Pareto* front of the wide color gamut display with our modified CFs and all the linewidths of the three primaries are set at 20nm, for both MVA and n-FFS modes. (d) Simulated color triangle of the wide color gamut QD-LCD (MVA mode).

The solid lines in Fig. 2(b) are the conceptual color filters we designed. In comparison with the commonly used color filters for TVs (dashed lines), our modified color filters exhibit a wider color gamut based on following two important design features: 1) The transmittance curves are much cleaner as the tails in the red and blue regions diminish; this is essential because these tails degrade the color purity of the primaries. 2) The transmission band of both blue and green color filters is narrowed to minimize the overlapping between different color channels. Figure 2(c) depicts the *Pareto* Front for MVA and n-FFS modes. With the proposed color filters and setting the linewidths of all three primary colors to 20nm, we can achieve ~97.6% of the Rec. 2020 color gamut in CIE 1931, or ~98.6% in CIE 1976. The *TLE* of MVA is ~40% lower than that of n-FFS. Such a wide color gamut display can reproduce most of the colors that Rec. 2020 demands [29]. If we inspect the color triangle in Fig. 2(d), we can determine that the color triangle overlaps well with the Rec. 2020 standard except that the green deviates slightly. Table 4 lists the optimized parameters for both MVA and n-FFS.

If we compare Tables 2-4, we can find the tradeoff between color gamut and *TLE* is quite significant. For example, for the n-FFS mode shown in Table 2 and Table 4, when the color gamut widens from 92.3% to 97.5%, which is 5.6% increase, the *TLE* drops from 24.6 to 18.3, which is 25.6% decrease in optical efficiency. Such a sacrifice may not be worth taking because power efficiency is a critical issue for all displays. For practical applications, we need to balance color gamut with optical efficiency. We will give a more detailed discussion in Sec. 5.

Meanwhile if we compare the optimized wavelengths in Table 4 to those listed in [7], which are optimized to cover the Pointer's Gamut, we find that these two results are quite close except for the green primaries. This similarity comes from the fact that Rec. 2020 is also designed to cover the Pointer's Gamut. As for the green primaries, they are a little bit different because of the greatly modified green color filter in our design.

Table 4. System parameters of the widest color gamut we can get with the modified color filters, for both MVA and n-FFS modes.

LC mode		MVA	n-FFS
Central Wavelength (nm)	Red	637.8	638.3
	Green	530.9	530.5
	Blue	469.1	467.6
<i>TLE</i> (lm/W)		12.1	18.3
Color Gamut		97.6%	97.5%

4. Wide color gamut RGB QLED

QLED has long been considered as a potential candidate for next generation display because it offers narrow linewidth and selectable central wavelength. Moreover, the device structure is similar to that of contemporary OLED. Consequently, QLED is also suitable for flexible displays and its manufacturing is compatible to OLED. Previously, QLEDs are regarded as a future technology because of its relatively low external quantum efficiency (EQE) and relatively short lifetime. Recently, with the demonstration of high EQE and long life quantum dots, there is renewed strong interest on QLED. Figure 3(a) shows the typical device structures of high efficiency RGB QLEDs. These structures are similar to those proposed in [14]. The efficiency and emission spectra of the RGB QLEDs can be calculated by the dipole model [30–32] and the simulation results agree well with experiments. If we assume that quantum efficiency and the charge balance is unity, the corresponding EQE for the RGB QLEDs are 17.2%, 16.5% and 17.7%, respectively. These results are quite close to the reported experimental data. In addition, if we know the real quantum efficiency and charge

balance of the device, we can get a better match between simulation and experiment. The calculated normalized emission spectra of the RGB QLEDs are shown in Fig. 3(b).

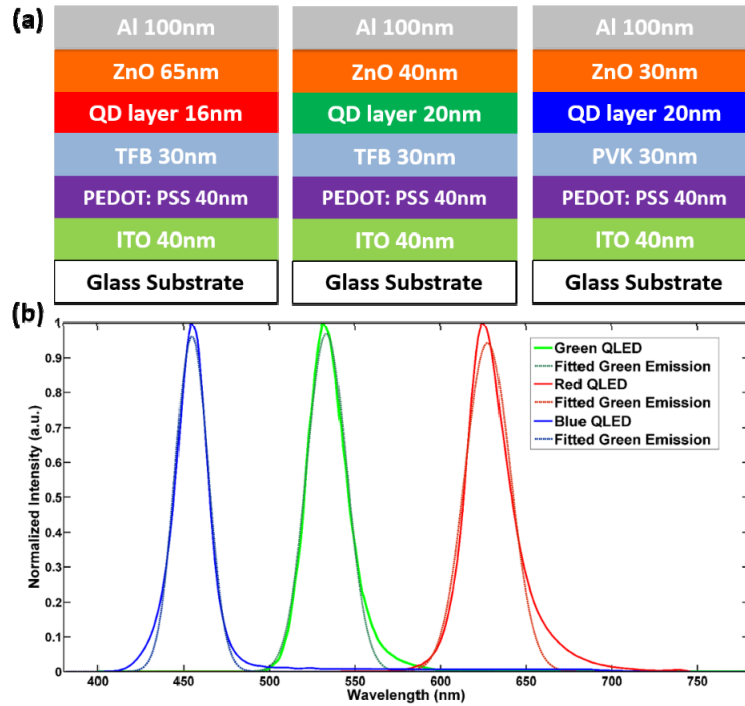


Fig. 3. (a) Device structures and (b) emission spectra of the RGB QLEDs.

From Fig. 3(b) we find that the emission spectrum of each QLED fits well with the Gaussian distribution; the R^2 values for all three curves are all larger than 99.7%. Here the RGB QLEDs shown in Fig. 3 can realize 85% of Rec. 2020, which is still insufficient. We can still optimize the color gamut coverage and LER simultaneously for the QLED. Results are shown in Fig. 4. The linewidths of the RGB QLEDs are 1) 30nm for RGB (blue curve; lower limit), 2) 30nm for red and green, and 20nm for blue (green curve, intermediate case), and 3) 20nm for RGB (red curve; upper limit). As expected, the green curve lies between the red and the blue curves.

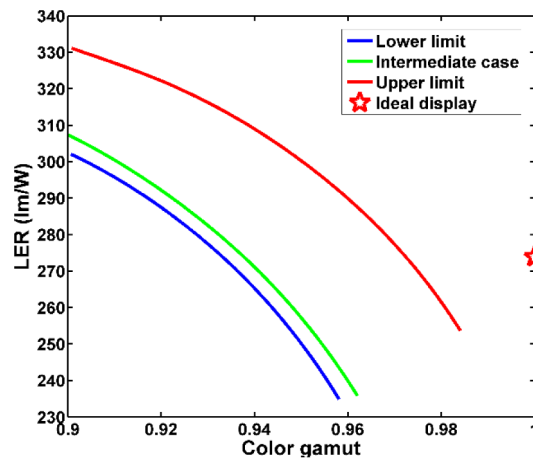


Fig. 4. The relationship between color gamut and LER for RGB QLEDs.

From Fig. 4, similar to QD-LCD, we cannot achieve 100% Rec. 2020 (ideal case) because of the linewidth of the RGB QLEDs. However, RGB QLEDs can easily achieve 95% of the Rec. 2020 standards even with a linewidth of 30nm because there is no crosstalk coming from color filters. If we compare the blue and red curves, we can easily find that at the same color gamut the *LER* is 13% higher for the QDs with 20nm linewidth. This suggests that for the EL case, developing QDs with a reasonably narrow linewidth (~20nm) is advantageous for both color gamut and efficiency. From Fig. 4, we can find the following best result that RGB QLEDs can get: when the central wavelength of the 20nm-linewidth RGB QLEDs is 634.3nm, 530.6nm and 465.8nm, respectively, we can get an optimized 98.4% color gamut (99.0% in CIE 1976) with a high *LER* of 252.8 lm/W. Such a wide color gamut can be regarded as ready to reproduce most of the colors that Rec. 2020 enables [29]. Compared to the ideal display (100% Rec. 2020 color gamut with three monochromatic light sources), the *LER* of our RGB QLED is still 7.7% lower. If we plot the color triangle in the CIE 1931 color space in Fig. 5, we can easily catch that the red and blue colors are quite close to the Rec. 2020 color primaries while the green color is still a little bit off. Similar to QD-enhanced LCD, if we can squeeze the linewidth of the RGB QLEDs to 10nm, then we can realize 99.5% of the Rec. 2020 color gamut with *LER* = 251.5 lm/W. However, it remains technically challenging to develop 10-nm-linewidth QDs.

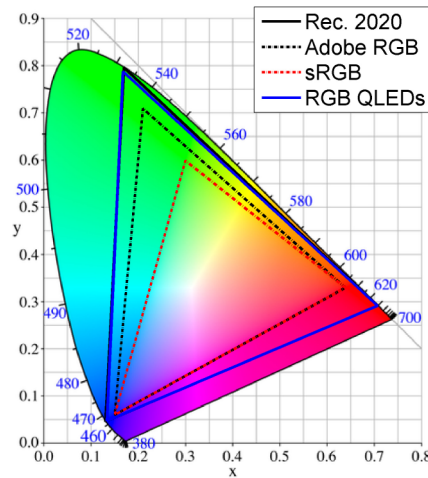


Fig. 5. Color gamut representation of the proposed RGB QLEDs.

5. Discussion

5.1. Color space selection

As we have briefly mentioned in Sec. 2, the selection of color space for calculating color gamut is quite important but sometimes misleading. For example, considering the RGB QLEDs shown in Fig. 3, the color gamuts in the CIE1931 and CIE1976 color space shown in Figs. 6(a) and 6(b) are 84.6% and 85.4%, respectively. The spectra of the RGB QLED are shown in Fig. 6(c) and the *LER* of the RGB QLED display is 290.8 lm/W. From Figs. 6(a) and 6(b), we can find that even though statistically speaking the color gamut in CIE 1931 and CIE 1976 is quite similar, the visual feeling is quite different. In Fig. 6(a), it seems that the QLEDs can well reproduce both red and blue, but not green. However, in CIE 1976 Chromaticity Diagram it seems that the QLED can better reproduce green than red and blue. To answer which representation is closer to reality, we convert the Rec. 2020 standard and the QLED color gamut to the CIELAB color gamut, and the results viewed down from the L axis is shown in Fig. 6(d). The wireframe color gamut is the Rec. 2020 standard and the solid color gamut is the color gamut of the QLED display, we can intuitively determine that the

maximum mismatch happens in the green color. This suggests the color gamut shown in CIE 1931 color space is more correlated to the 3D color perspective model, which matches the conclusion stated in [16]. Under this consideration, we decide to calculate color gamut in CIE 1931. For real products, we have to analyze the color difference of the display quantitatively and further calculate the volume-coverage ratio.

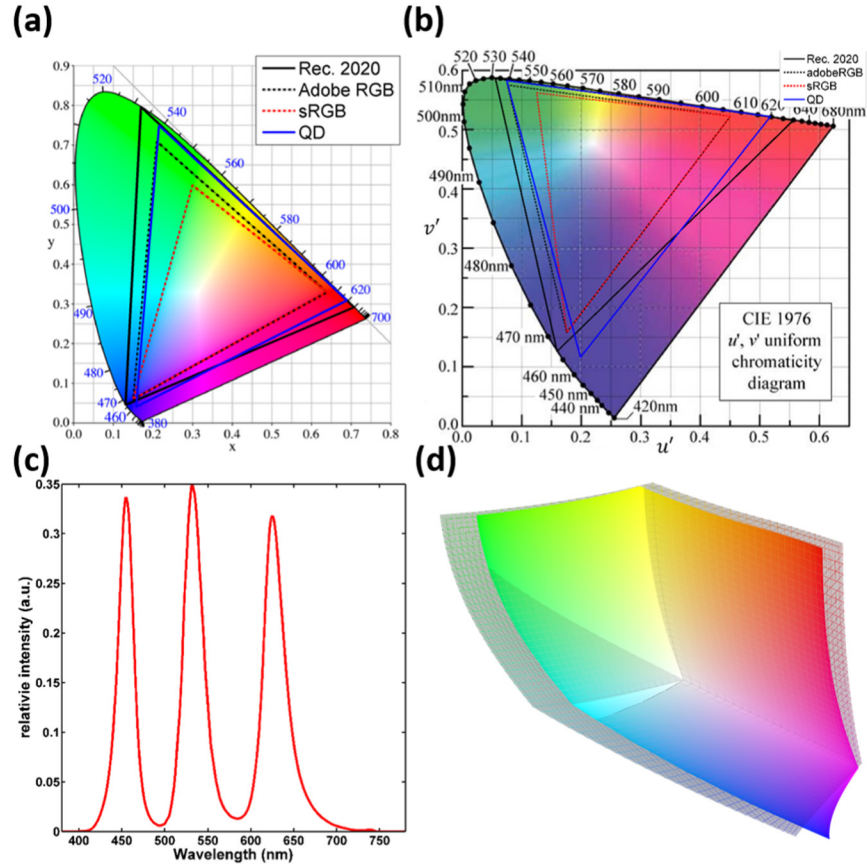


Fig. 6. Color gamut of a RGB QLED in (a) CIE 1931 and (b) CIE 1976; (c) emission spectra of the RGB QLEDs and (d) color gamut comparison of Rec. 2020 and the QLED display in CIE LAB, the wireframe color gamut is Rec. 2020 and the solid color gamut is the RGB QLED.

5.2. Angular performance of QD-LCD and RGB QLEDs

Color shift at an off-axis angle is a critical issue. For an QD-LCD, the angular performance is primarily determined by the birefringence of the LC material [33]. Here we demonstrate that with two wide-view LC modes: 1) two-domain (2D) n-FFS for smart phones and 2) 4D MVA for TVs. From Figs. 7(a) and 7(b), the color shift of each RGB primary color is rather small and the blue has the largest color shift. For the worst scenario, the color shift ($\Delta u'v'$) of the blue color stays below 0.01 at 80° viewing angle. As long as $\Delta u'v' < 0.02$, it is difficult for human eye to notice the difference [34]. Thus, such an LCD has negligible color shift. However, the color shift for the white color is much larger. For the 2D n-FFS mode, the color shift is still smaller than 0.02 at 80° for RGB and white. The situation for 4D MVA is drastically different. For the white color, the color shift is approaching 0.04 at 80° viewing angle. The small color shift for the RGB primaries means that we do not have to worry about the color gamut shrink at large viewing angle. While the small color shift for the white color

in 2D n-FFS indicates that we can avoid the usage of color mixing films [35]. The reason that 4D MVA has a larger color shift than 2D n-FFS is that for 4D MVA the LC directors are vertically tilted, while for 2D n-FFS the LC directors are rotated in plane. In the former case, it is easier to observe the birefringence effect at off-axis. In commercial TV products, 8D MVA is commonly used to mitigate the color shift [23].

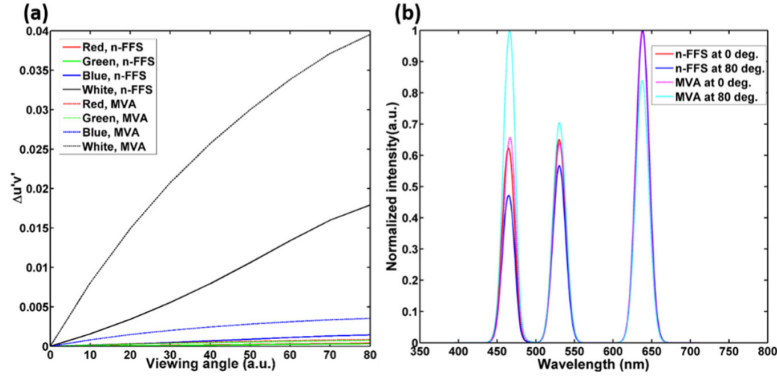


Fig. 7. (a) Color shift of QD-LCDs for 2D n-FFS and 4D MVA, and (b) the normalized output spectra of the QD-LCD at different viewing angle.

As for the RGB QLEDs, color shift comes from cavity effect [36]. The angular performance of RGB QLED can also be evaluated by the dipole model. For example, for the RGB QLED mentioned in Fig. 3, the angular dependent emission spectra are shown in Fig. 8(a) and we can find that each individual spectrum remains quite narrow even at a large off-axis angle. From Fig. 8(b), the color shift of each individual color R, G and B is quite small. The largest color shift $\Delta u'v'$ for blue is still smaller than 0.002, which is 10X below the distinguishable level. As for the combined white color, $\Delta u'v'$ reaches 0.02 at 65°. The reason for the relatively large color shift for the white color can be deduced from Eq. (6) and Fig. 8(a). As demonstrated in Eq. (6), the white color is optimized for the normal viewing angle. For the off-axis angle, the emission pattern drops differently for different colors, thus Eq. (6) no longer matches the system's white point. To reduce color shift, we can optimize the QLED cavities to tune the angular emission pattern. However, this approach is quite unintuitive and it is difficult to predict how the angular emission pattern changes with different QLED stack configuration. Another way is to use optical diffusers, microstructures or other kinds of color mixing films to mitigate the color shift. This approach has been widely used in contemporary LCDs [35].

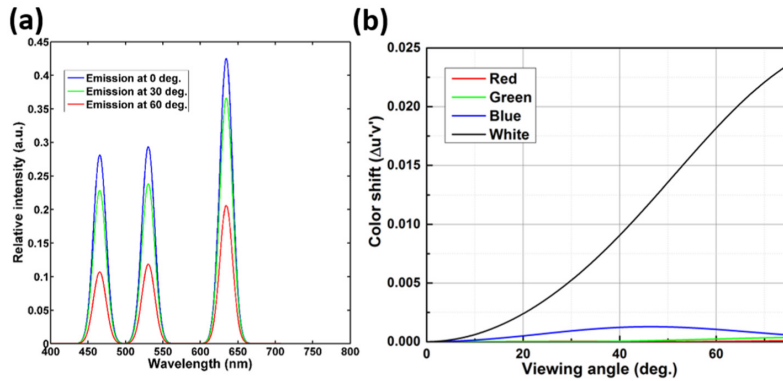


Fig. 8. (a) Angular dependent emission spectra for the RGB QLED; and (b) Color Shift of the RGB QLEDs.

5.3. Comparing QD-LCD with red and green phosphors embedded LCD

Besides QDs, two-phosphor LEDs (2p-LED, i.e. blue LED pumping red and green phosphors) have also attracted much attention because of their excellent reliability and low cost. Figure 9(a) shows the emission spectra of such a 2p-LED [10, 37]. From Fig. 9(a), the green and red emission spectra are relatively broad as compared to quantum dots. Our simulation results in Fig. 9(b) show that for this 2p-LED backlit LCD system with the color filters designed for TV, it covers 90% of the Adobe RGB and 67% of the Rec. 2020, and the *TLE* is 21.7 lm/W for the n-FFS mode and 15.6 lm/W for the MVA mode. Therefore, we find that theoretically QD offers wider color gamut and higher optical efficiency than 2p-LED. However, contemporary red and green phosphors can be deposited on top of the blue LED chip to form a white LED [38], whereas for red and green QDs, it is still not mature to place them on the blue LED chip [39] because of the material reliability issue. The “on edge” and “film” approaches for QDs are not as efficient as the white LED with 2p phosphors because of the longer optical path.

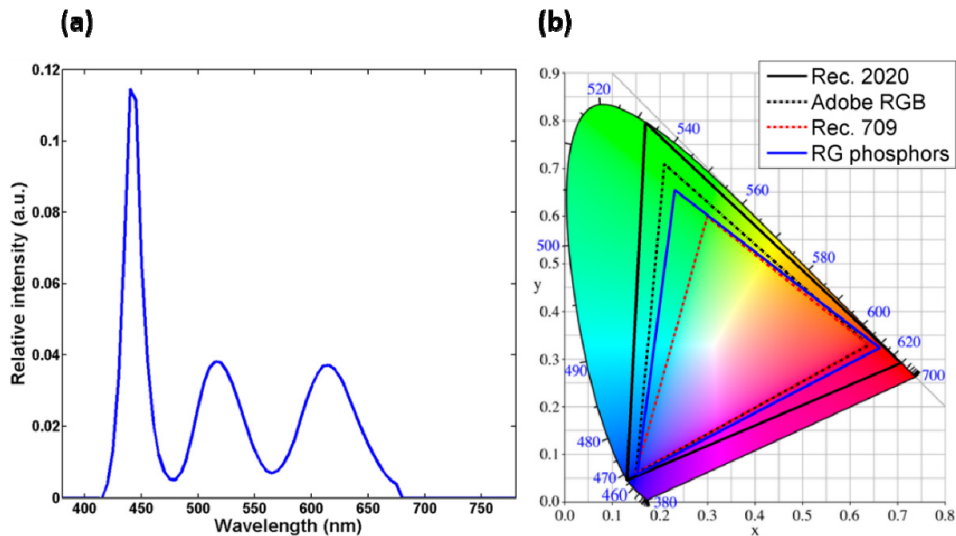


Fig. 9. (a) The spectra of the RG phosphor embedded LCD and (b) its color triangle.

As we mention earlier, for both QLED and QD-LCD, widening color gamut is associated with reduced optical efficiency. However, this does not necessarily indicate that for the same input power, a wider color gamut display always suffers from lower brightness. Another entoptic phenomenon called the Helmholtz–Kohlrausch (HK) effect [40] has to be taken into consideration as well, that is, a more saturated color produced by the wide color gamut display is perceived brighter. The Perceived Quality Metric (PQM) [41] has been proposed to describe the display quality quantitatively, as Fig. 10 depicts. This figure describes how display quality is affected by both luminance and color area. In this isoquality figure, the line at the upper right corner has the best perceived quality, and points on the same line is considered as equal quality. Here color area is defined similar to Eq. (1), except that $A_{standard}$ here is the Adobe RGB and the color area is calculated in the CIE 1976 color space. Taken our wide color gamut MVA model in Table 4 as an example, the color area is 149.2% (the red vertical line), while for the 2p-LED lit LCD, the color area is 106.9% (the blue vertical line). From Fig. 10, we find that a 300 cd/m² QD-LCD is perceived equivalent to a 435 cd/m² 2p-LED lit LCD. The luminance requirement is only about 69.0%. Considering the *TLE* of the two devices (12.1 vs 15.6), this means the wide color gamut display does not necessarily look as dim as its efficiency indicates.

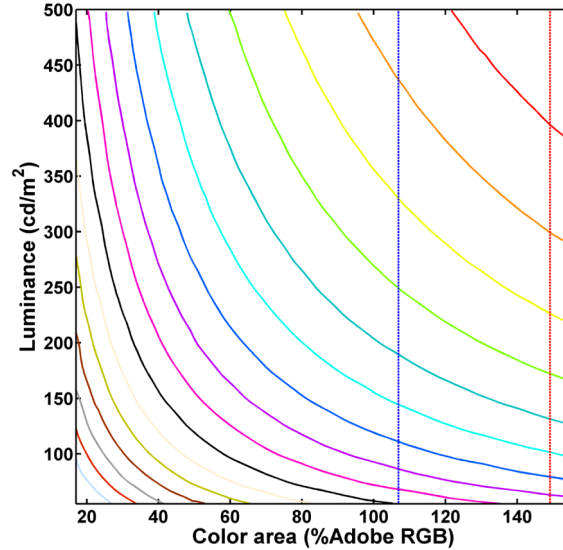


Fig. 10. Isoquality curves of the perceived quality metric.

6. Conclusion

We have analyzed how to obtain a wide color gamut display for both QD-LCD and RGB QLEDs. The relationship between optical efficiency and color gamut is explained for both approaches. For QD-LCDs, we can easily achieve more than 90% of the Rec. 2020 standard through spectral optimization with contemporary commercial color filters. However, to realize more than 97% of Rec. 2020, color filters have to be modified and *TLE* sacrificed. The angular performance of QD-LCDs is determined by the LC mode. With 2D n-FFS mode, the combined white color exhibits an indistinguishable color shift. As for RGB QLEDs, it can easily achieve Rec. 2020 through spectral optimization, and the angular performance of the QLEDs is mainly governed by the QLED cavity. For each primary color, the color shift is negligible; but for the combined white color, the color shift might still be noticeable.

Acknowledgments

The authors are indebted to Prof. Jiun-Haw Lee of National Taiwan University for helpful information and stimulated discussion, and AFOSR for partial financial supports under contract No. FA9550-14-1-0279.